Mon. Not. R. Astron. Soc. **326,** 995–1006 (2001)

The X-ray spectra of optically selected Seyfert 2 galaxies: are there any Seyfert 2 galaxies with no absorption?

A. Pappa,[1★†] I. Georgantopoulos,[2] G. C. Stewart[1] and A. L. Zezas[1‡]
[1]*Department of Physics and Astronomy, University of Leicester, Leicester, LE1 7RH*
[2]*Institute of Astronomy and Astrophysics, National Observatory of Athens, Lofos Koufou, Palaia Penteli, 15236, Athens, Greece*

Accepted 2001 April 20. Received 2001 April 5; in original form 2000 July 4

ABSTRACT

We present an X-ray spectral analysis of a sample of eight bona fide Seyfert 2 galaxies, selected on the basis of their high [O III]λ5007 flux, from the Ho et al. spectroscopic sample of nearby galaxies. We find that, in general, the X-ray spectra of our Seyfert 2 galaxies are complex, with some of our objects having spectra different from the 'typical' spectrum of X-ray selected Seyfert 2 galaxies. Two (NGC 3147 and 4698) show no evidence for intrinsic absorption. We suggest that this is a result of the fact that when the torus suppresses the intrinsic medium and hard energy flux, underlying emission from the host galaxy, originating in circumnuclear starbursts, and scattering from warm absorbers contributes in these energy bands more significantly. Our *ASCA* data alone cannot discriminate whether low-absorption objects are Compton-thick active galactic nuclei (AGNs) with a strong scattered component or lack an obscuring torus. The most striking example of our low absorption Seyfert 2 is NGC 4698. Its spectrum could be explained by either a dusty warm absorber or a lack of broad-line clouds so that its appearance as a Seyfert 2 is intrinsic and not a result of absorption.

Key words: galaxies: active – galaxies: Seyfert – galaxies: starburst – X-rays: galaxies.

1 INTRODUCTION

The discovery of hidden Seyfert (Sy) 1 nuclei in many Seyfert 2 galaxies has given much support to the unified theories of Seyferts (e.g. see Antonucci et al. 1993 for NGC 1068). According to the current unification models, both are identical objects which possess a core-central black hole, accretion disc, broad-line region and a thick molecular torus. Objects observed within the opening angle of the torus are classified as Seyfert 1 objects, whereas those seen at angles intersecting the torus appear as Seyfert 2 sources. Around the core is ionized gas (warm scatterer) which scatters the primary emission. In some cases nuclear starburst regions have been observed. It should be pointed out that the unified theories explain the differences between type 1 and type 2 Seyferts (and active galaxies in general) phenomenologically, attributing any difference to orientation effects only. The X-ray data support the above picture. The X-ray spectra of X-ray selected Seyfert 2 galaxies (e.g. Turner & Pounds 1989; Smith & Done 1996; Turner et al. 1997) show column densities much higher than those of Seyfert 1 objects. These columns completely block the soft X-ray flux but become transparent to energies $\geqslant 2$ keV. Thus X-rays prove to be a powerful tool for the study of the type 2 (obscured) objects, because X-ray photons can penetrate the obscuring medium and reveal the core to the observer.

Some objects, although classified as Seyfert 2 galaxies (e.g. NGC 1068 and Circinus; see Matt et al. 1997, 1999 respectively), appear to have no excess absorption. It has been shown that in such cases the direct component in the 2–10 keV range is suppressed as a result of the fact that the torus is optically thick to Compton scattering, thus the hard X-ray photons in the 2–10 keV range are shifted to lower energies and are eventually absorbed after a few scatterings. In X-ray astronomy terminology these objects are classified as Compton-thick Seyfert 2 galaxies. In such cases the emission from the nucleus can be inferred from the photons scattered from the warm scatterer and the inner surface of the torus itself (cold scatterer). Therefore Compton-thick objects can show low obscuration below 10 keV. *BeppoSAX* observations with the Phoswich Detector System (PDS) have revealed that a power-law emerges through a high column density ($>10^{24}\,\mathrm{cm}^{-2}$) above 10 keV in several such cases. In such cases the obscuration is large enough to completely block the direct emission, leaving a low 'pseudo-column' below 10 keV, but small enough to allow transmission above this energy. However, in some cases the column is so high ($>10^{25}\,\mathrm{cm}^{-2}$) that the emission is not detected with the PDS. In addition, the observed equivalent width of the K_α iron line increases as it is measured against a suppressed continuum.

★E-mail: apa@roe.ac.uk
†Present address: Institute for Astronomy, Royal Observatory, Blackford Hill, Edinburgh EH9 3HT.
‡Present address: Harvard-Smithsonian Center for Astrophysics, 60 Gardes Street, Cambridge, MA 02138, USA.

Until recently, Seyfert 2 studies were restricted to relatively X-ray bright Seyfert 2, mainly taken from all-sky X-ray surveys, leading to a bias in favour of galaxies with low $N_{\rm H}$. Maiolino et al. (1998) studied a sample of X-ray weak Seyfert 2 galaxies selected by their [O III]λ5007 flux and found that the average obscuration of type 2 active galactic nuclei (AGNs) is much higher than that derived by the former X-ray studies. This is because the [O III]λ5007 flux is produced above or below the torus and therefore can be considered to represent the central engine and thus provide us with an unbiased sample of Seyfert 2 galaxies. Recently, Risaliti, Maiolino & Salvati (1999) studied a large sample of [O III]λ5007 selected late-type Seyfert galaxies (Seyfert 1.8, 1.9, 2.0; [O III]λ5007 $> 40 \times 10^{-14}$ erg s^{-1} cm^{-2}). The galaxies came from Maiolino & Rieke (1995), complete with NGC 1808. Using X-ray data from the literature (with the exception of five objects, where the authors analysed the data), they showed that the average column density for these objects is $N_{\rm H} = 10^{23.5}$, with all the Seyfert 2 galaxies being obscured by columns with $N_{\rm H} > 10^{22}$ cm^{-2}, giving strength to the simple model proposed by the unified theories. Furthermore, they showed that about half of them are Compton-thick ($N_{\rm H} > 10^{24}$ cm^{-2}) and they confirmed that intermediate type 1.8–1.9 Seyferts are characterized by an average $N_{\rm H}$ distribution lower than that of the genuine Seyfert 2 galaxies.

Although the above standard model describes the spectrum of most Seyferts very well, examples of Seyfert 2 galaxies were found recently which challenge the unification scenarios. These show no intrinsic absorption (see, for example, Ptak et al. 1996 for NGC 3147 and Bassani et al. 1999 for NGC 7590) while their high $f_{\rm HX}/f_{\rm [O_{III}]}$ ratios are inconsistent with the idea of being Compton-thick objects (see Bassani et al. 1999). The peculiar spectra of these Seyfert 2s could be explained, for instance, either by the absence of a broad-line region or by a high dust to (∼ neutral) gas ratio . In the former case, their appearance as Seyfert 2s is intrinsic and not a result of absorption. The lack of absorbing columns in these galaxies raises important questions about the validity and universality of the standard AGN unification schemes. The distribution of the absorbing columns in AGNs is also vital for models for the synthesis of the cosmic X-ray background (XRB; e.g. Comastri et al. 1995). It is evident that the range of column densities of the absorbing material, its structure and geometry remain yet unconstrained and need to be determined with larger samples of galaxies selected in different wavebands.

In this paper, we present a comprehensive and uniform X-ray analysis with *ASCA* data of eight optically selected Seyfert 2 galaxies from the spectroscopic sample of Ho et al. (1997). While a few of the objects analysed here have been retrieved from the public *ASCA* database, some are presented here for the first time (NGC 1167, 2273, 3486 and 4698). Our goal is to explore the validity of the standard model and study the distribution of absorbing columns in a sample with very accurately defined optical properties, bona fide Seyfert 2. This paper is divided as follows: in Section 2 we introduce our sample; in Section 3 we describe our analysis method; in Section 4 we present the results of the spectral analysis; in Section 5 we discuss our results of the individual objects; in Section 6 we discuss our results and in Section 7 we summarize our main observational results.

2 THE DATA

We present an analysis of eight optically selected Seyfert 2 galaxies observed with the *ASCA* satellite. The list of the data is presented in Table 1. The data come from both our own proprietary observations and from the *ASCA* archive. Our galaxies are taken from the Ho et al. (1997) spectroscopic sample of nearby galaxies. This sample contains objects selected from the Revised Shapley-Ames Catalogue of Bright Galaxies (RSA; Sandage & Tammann 1981) with magnitude limit $B_\tau = 12.5$ mag in the northern ($\delta > 0°$) sky. As high signal-to-noise and moderate- to high-resolution optical spectroscopy has been obtained for this sample, very accurate spectroscopic classifications exist for all galaxies. As a consequence we can be confident that all our objects are bona fide Seyfert 2 galaxies. Our eight objects are selected on the basis of their high [O III]λ5007 flux. Some of our objects (see Table 1) have been previously analysed by other authors in the hard X-ray band. However, here we re-analyse the data in order to present a uniform, comprehensive analysis of the brightest [O III]λ5007 selected Seyfert 2, for which X-ray data were/became available in the Ho et al. (1997) sample. An [O III]λ5007 selected sample should be relatively free from the selection effects and biases that might appear through X-ray or other optical selection, such as intrinsic absorption or differences in viewing angle (Ueno et al. 1998). For five of the sources we were able to perform spectral analysis. For the other three (NGC 1167, 1667 and 3486), insufficient X-rays were detected for a full spectral analysis and we restrict ourselves to a hardness ratio analysis.

Table 1. The *ASCA* Seyfert 2 sample. The columns contain the following information: (1) the source name; (2) the sequence number of the observation; (3) and (4) optical position of the object; (5) the exposure time for SIS-0 in ks; (6) the source redshift; (7) the line-of-sight Galactic hydrogen column density; (8) references to the previously published hard X-ray data.

(1) Name	(2) *ASCA* sequence	(3) RA[a] (J2000)	(4) Dec.[a] (J2000)	(5) SIS-0 exp. (ks)	(6) z [b]	(7) $N_{\rm H}$(Gal) ($\times 10^{21}$ cm^{-2})	(8) References
NGC 1167	77072000	03 01 42.4	+35 12 21	38	0.016495	1.14	–
NGC 1667	71032000	04 48 37.1	−06 19 12	14.5	0.015167	0.55	1,2
NGC 2273	74039000	06 50 08.7	+60 50 45	34	0.006241	0.68	3
NGC 3079	60000000	10 01 57.8	+55 40 47	29	0.003753	0.08	4
NGC 3147	60040000	10 16 53.6	+73 24 03	23	0.009407	0.36	5
NGC 3486	77074000	11 00 23.9	+28 58 30	41.3	0.002272	0.19	–
NGC 4698	77073000	12 48 23.0	+08 29 14	40.5	0.003342	0.19	–
NGC 5194 (M51)	60017000	13 29 52.35	+47 11 53.8	30.5	0.001544	0.16	6

Notes. [a] Units of right ascension are hours, minutes and seconds. Units of declination are degrees, arcminutes and arcseconds. [b] From the NASA Extragalactic Database (NED). REFERENCES. 1: Ueno et al. (1997). 2: Turner et al. (1997). 3: Maiolino et al. (1998). 4: Ptak et al. (1999). 5: Ptak et al. 1996. 6: Terashima et al. (1998).

3 DATA REDUCTION

We utilized both the *ASCA* gas imaging spectrometer (GIS) and solid-state imaging spectrometer (SIS) data. We used the standard 'Revision 2' processed data from the Goddard Space Flight Center (GSFC) and data reduction was performed using FTOOLS. For GIS data we used a circular source region centred on the source. Background counts were estimated from source-free annuli centred on the source cell. Because of calibration differences between the four SIS chips, we limited our analysis to the on-source chip for each SIS. We used a circular extraction cell of 3–4 arcmin in radius. In cases where the source was centred close to the gap between the chips, we followed the process described in the *ASCA* ABC guide (Yaqoob 1997). The background was estimated using rectangular regions at the source chip, excluding the source. In the case of NGC 2273 where an additional serendipitous source close to the galaxy is detected, we used a circular source region of 1.5 arcmin in radius for both the GIS and SIS in order to minimize any contamination by the nearby source.

4 SPECTRAL ANALYSIS

The spectral analysis was carried out using XSPEC v10. We bin the data so that there are at least 20 counts in each bin (source plus background). The quoted errors to the best-fitting spectral parameters are 90 per cent confidence regions for one parameter of interest ($\Delta\chi^2 = 2.71$). We performed spectral fitting, allowing the normalization for the SIS and GIS detectors to vary. The fluxes and luminosities given in the tables are referred to the GIS data. Throughout this paper, values of $H_o = 75\,\mathrm{km\,s^{-1}\,Mpc^{-1}}$ and $q_o = 0.5$ are assumed. From our analysis, we exclude all data below 0.8 keV because of the uncertainties in the calibration matrices (see George et al. 1998 for a discussion on this). We apply relatively simple spectral models, so as to describe the properties of the whole sample in the context of the unified model. We apply all the models to all the data sets even though the most complex models may not be required in some cases. Where fits gave us absorption values consistent with the Galactic column density or lower we have fixed the column to the Galactic value. The latter was determined using the FTOOLS program, which utilizes a map based on 21-cm measurements and has resolution of about 0.7 degrees (see Dickey & Lockman 1990).

4.1 Building the standard model

We have used the four major components of the 'standard model' in steps:

(i) we first apply a single power-law with absorption, if required, to all of our objects,

(ii) we then add a Gaussian line representing the iron K_α emission,

(iii) we add a second power-law component representing scattered emission, and finally

(iv) a Raymond-Smith component at low energies representing a star-forming component is added to the data.

4.1.1 Single power-law model

According to the current theories, the primary ultraviolet (UV) and soft X-ray photons produced by the disc are Compton scattered by a medium of hot electrons (~50 keV) and re-radiated at hard energies. Such a process can produce a power law with an index of $\Gamma \sim 1.9$, in agreement with observational results, which suggests that the intrinsic X-ray spectrum of Seyfert 1 galaxies is well represented by a power law with a 'canonical' spectral index with $\Gamma \sim 1.9$. In the case of Seyfert 2 galaxies, where our line of sight intersects the torus, we expect the spectrum to show a low-energy cut-off as well. We thus fit the data with a power-law model $N(E)\,\mathrm{d}E \alpha E^{-\Gamma}\,\mathrm{d}E$, where $N(E)$ is the photon number density at energy E. The photoelectric absorption $A(E)$ is parametrized by $A(E) = \exp[-N_\mathrm{H}\sigma(E)]$ where N_H is the equivalent hydrogen column and $\sigma(E)$ is the photoelectric cross-section taken from Morrison & McCammon (1983). Fig. 1 shows the data and the data/model ratio after this model was fitted to each object. Rather unexpectedly, this model does provide an acceptable fit in two cases, where the absorption needed is either the Galactic value (NGC 3147) or relatively low (NGC 4698). An absorbed power-law model is clearly rejected by the NGC 2273 and M51 data. The model parameters are shown in Table 2. For the cases of M51, where the obtained spectral slope is unphysically steep, and NGC 2273, where the slope is rather flat, we also fitted the model with the slope fixed at the nominal value of $\Gamma = 1.9$, for comparison.

4.1.2 Iron K_α line

Strong evidence supporting the presence of an accretion disc in the vicinity of a black hole has been given by the detection of an asymmetric broad emission line at a rest energy of ~6.4 keV in the Seyfert 1 galaxy MCG-6-30-15. This is interpreted as K_α iron emission originating by fluorescence in the very inner parts of an accretion disc, $3R_\mathrm{S} \leqslant R \leqslant 10R_\mathrm{S}$, about a massive black hole of Schwarzschild radius R_S (Tanaka et al. 1995). The profiles and intensities of the iron lines are expected to be complex (asymmetric, double peaked) but the sensitivity of the current detectors cannot provide us with such detailed profiles for the majority of the observed objects. In the Seyfert 2 galaxies, reprocessing of the nuclear radiation by the obscuring torus may also contribute to the line flux. The mean equivalent width for a sample of Seyfert 2 galaxies studied with *ASCA* is 363 ± 254 eV (Gilli et al. 1999).

Some of our objects show line-like residuals in the 6–7 keV energy range, providing evidence for an iron line, which we parametrize by a Gaussian line. For the purposes of our study the width of the line is fixed at $\sigma = 0.01$ keV. This is smaller than the instrumental response and thus is effectively monochromatic. The addition of an iron line provides a significantly better fit (at $\geqslant$99 per cent confidence) for three of our objects (NGC 2273 and 3147, and M51), although we note here that the line equivalent widths determined may be strongly affected by the continuum shape and may be unphysical. The energy of the iron line is consistent with that expected for cold iron for all of our objects in which the line is detected. No line was detected in the spectra of NGC 3079 or 4698, for which we give the 90 per cent upper limits. The results are shown in Table 3.

4.1.3 The scattering model

According to the unified model, we expect that a fraction of the primary emission should be Thomson scattered into our line of sight by a photoionized medium. The scattered spectrum has the same shape as the incident spectrum. We note that in this work the term 'scattering' always refers to scattering off the warm photoionized medium. Optical polarimetric observations (Tran

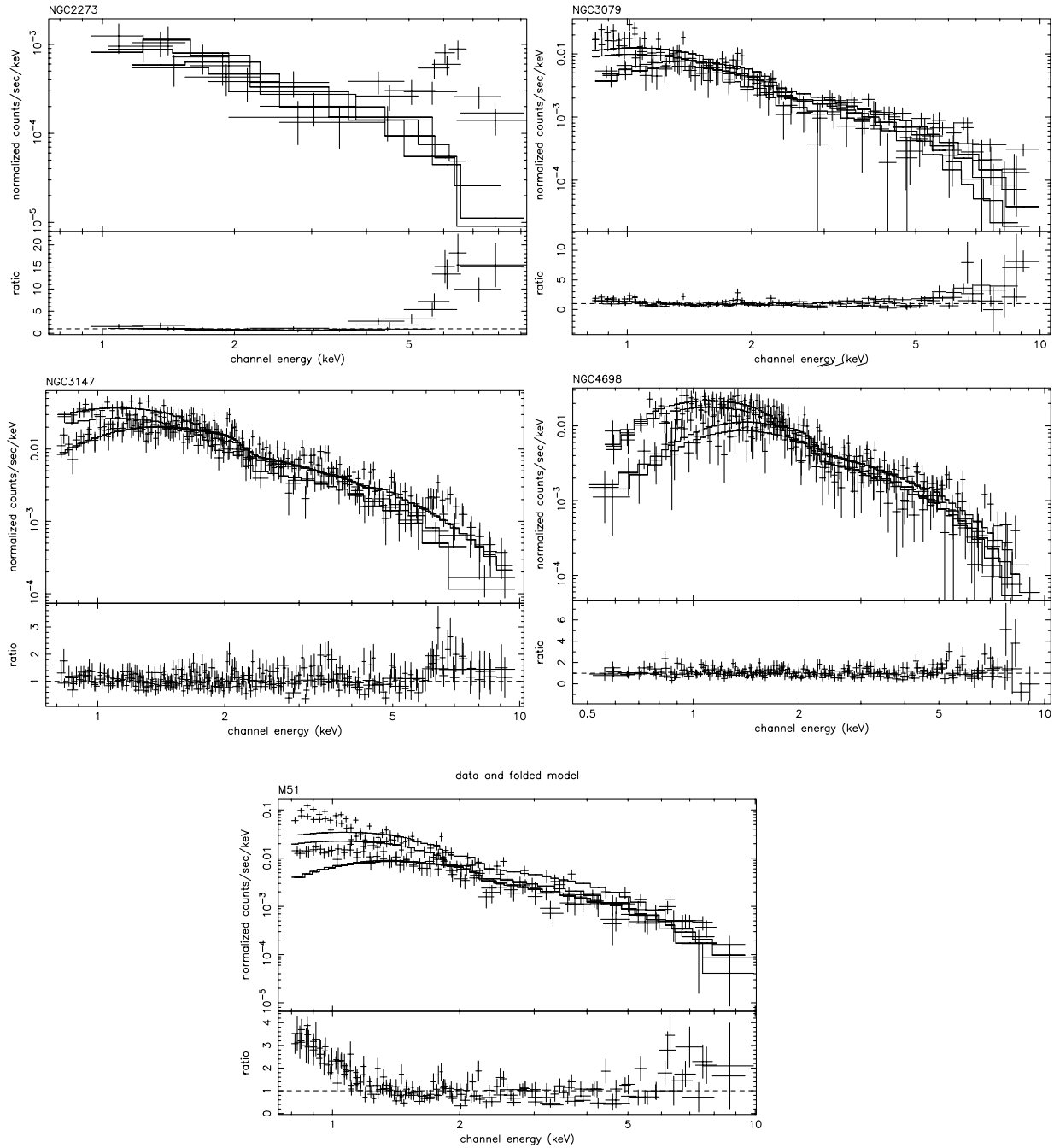

Figure 1. The single power-law model. The top section of each panel shows the data with the model and the bottom section of each panel shows the data/model ratio. In the bottom part of the panels the spectral features are clear.

1995) have shown that up to ∼10 per cent of the primary emission is scattered. The above scenario can be modelled using two power laws with the same photon index but different normalizations and absorptions. The results are shown in Table 4. Again the energy of the line is consistent with the expected 6.4 keV. For M51, we note that the obtained slope is unphysically steep and, although the fit has been improved, the model does not describe the data adequately. For NGC, 4698 although we obtain a good fit, the normalizations of the two power-law components are comparable, and neither component requires any absorption below 10 keV. In the case of NGC 3147 the column density is too high to be properly constrained in the *ASCA* energy range. Finally, in the case of NGC 2273, the normalizations of the scattered power-law component is almost two orders of magnitude lower than that of the primary power-law component, suggesting ∼2 per cent scattered flux, in agreement with what it is typically found to be for the obscured Seyfert galaxies (Sy 1.9–2.0).

4.1.4 Composite model

Infrared (Maiolino et al. 1995) and X-ray studies of Seyfert 2 galaxies (Turner et al. 1997) show that their host galaxies tend to have energetic starburst regions. Indeed some of our objects show line-like residuals at soft energies, suggesting thermal emission

Table 2. Single power-law model.

Name	Γ	$N_{\rm H}$ ($\times 10^{21}\,{\rm cm}^{-2}$)	$f_{(2-10\,{\rm keV})}{}^{a}$	$L_{(2-10\,{\rm keV})}{}^{b}$	χ^2/d.o.f.
NGC 2273	$-0.55^{+0.11}_{-0.11}$	0.68g	0.9	0.65	82.92/22
	1.9f	5.86	0.18	0.14	117.47/22
NGC 3079	$1.93^{+0.12}_{-0.12}$	0.08g	0.74	0.20	228.06/143
NGC 3147	$1.82^{+0.05}_{-0.06}$	0.36g	1.63	2.76	289.22/285
NGC 4698	$1.91^{+0.14}_{-0.14}$	$0.81^{+0.82}_{-0.78}$	1.04	0.22	243.90/250
M51	$3.07^{+0.06}_{-0.06}$	0.16g	0.35	0.02	568.88/178
	1.9f	0.16g	0.90	0.04	848.21/179

Notes. g indicates that the $N_{\rm H}$ is set to the Galactic value, whereas f indicates that the parameter value is frozen. [a]Observed 2–10 keV flux in units of $10^{-12}\,{\rm erg\,s^{-1}\,cm^{-2}}$. [b]Unobscured 2–10 keV luminosity in units of $10^{41}\,{\rm erg\,s^{-1}}$, corrected for absorption quoted in column 3.

Table 3. Power-law plus iron line.

Name	Γ	$N_{\rm H}$ ($\times 10^{21}\,{\rm cm}^{-2}$)	EW (eV)	$f_{2-10\,{\rm keV}}{}^{a}$	$L_{2-10\,{\rm keV}}{}^{b}$	χ^2/d.o.f.
NGC 2273	$1.09^{+0.43}_{-0.32}$	0.68g	9080^{+7000}_{-4500}	0.54	0.41	33.32/20
NGC 3079	$2.02^{+0.13}_{-0.11}$	0.08g	<2600	0.84	0.22	217.71/141
NGC 3147	$1.80^{+0.10}_{-0.05}$	0.36g	593^{+288}_{-223}	1.67	2.82	267.02/283
NGC 4698	$1.91^{+0.12}_{-0.10}$	$0.95^{+0.36}_{-0.42}$	<425	1.04	0.21	243.89/248
M51	$2.90^{+0.05}_{-0.05}$	0.16g	5520^{+1515}_{-1516}	0.53	0.02	532.33/176

Notes. g indicates that the $N_{\rm H}$ is set to the Galactic value. [a]Observed 2–10 keV flux in units of $10^{-12}\,{\rm erg\,s^{-1}\,cm^{-2}}$. [b]Unobscured 2–10 keV luminosity in units of $10^{41}\,{\rm erg\,s^{-1}}$, corrected for absorption quoted in column 3.

Table 4. Scattering model.

Name	Γ	$N_{\rm H}$ ($\times 10^{21}\,{\rm cm}^{-2}$)	EW (eV)	$f_{2-10\,{\rm keV}}{}^{a}$	$L_{2-10\,{\rm keV}}{}^{b}$	χ^2/dof
NGC 2273	$1.78^{+0.61}_{-0.27}$	982^{+196}_{-433}	555^{+4000}_{-520}	1.11	7.80	14.28/18
NGC 3079	$2.20^{+0.30}_{-0.20}$	950^{+525}_{-117}	<3000	1.13	0.21	192.18/140
M51	$4.40^{+0.36}_{-0.21}$	$64.7^{+8.8}_{-8.0}$	4100^{+2300}_{-2110}	0.60	0.06	298.81/174

Notes. [a]Observed 2–10 keV flux in units of $10^{-12}\,{\rm erg\,s^{-1}\,cm^{-2}}$. [b]Unobscured 2–10 keV luminosity in units of $10^{41}\,{\rm erg\,s^{-1}}$, corrected for absorption quoted in column 3.

arising from hot gas. Thus we utilize an emission spectrum from hot, diffuse gas (Raymond model in XSPEC) to model the starburst component, along with a single power law to account for the hard photons. The temperature is set to be $\leqslant$1.0 keV, in order to constrain the starburst contribution to the soft band. We fit NGC 3079 and M51 with this model because these galaxies show evidence for thermal emission. In the case of M51, the thermal component is absorbed by the Galactic column, whereas in NGC 3079, excess absorption is required. This model gives a good fit for both galaxies (see Table 5).

4.2 The Compton-thick models

If the column density exceeds $\sim 10^{24}\,{\rm cm}^{-2}$, the obscuring medium is optically thick to Compton scattering and thus the primary emission is suppressed and we only observe the scattered emission from either the warm matter or the inner surface of the torus itself. For the latter we use the term 'reflection'. Here we will consider the case where the Compton reflection from the inner surface of the torus dominates the observed emission in the 2–10 keV energy band. We therefore utilize the PEXRAV model in XSPEC, which describes reflection occurring from a slab of neutral material subtending a solid angle of 2π sr to an X-ray point source located above the slab to account for the total hard X-ray emission, and a power law to represent the soft emission. For the purpose of this study we consider that the slope of the underlying power-law spectrum is 1.9, and assume Galactic absorption. The normalization of the reflection is given by $R = \Omega/2\pi$, where Ω is the solid angle subtending by the reflector. However, as we cannot directly measure the intensity of the intrinsic power law which is being reflected, the value of R that we obtain is not physically meaningful. Therefore we define the ratio $A = R \times f_{(2-10\,{\rm keV})}/f_{(2-10\,{\rm keV})\rm sc}$ as an indicator of the fractional contribution that would have been made to our observed spectrum after correction for absorption by the PEXRAV reflector. $f_{(2-10\,{\rm keV})}$ is the flux that would have been produced by the underlying spectrum in

Table 5. Composite model.

Name	Γ	N_H ($\times 10^{21}$ cm^{-2})	KT	EW (eV)	$f_{2-10\,keV}$[a]	$L_{2-10\,keV}$[b]	χ^2/dof
NGC 3079	$0.79^{+0.31}_{-0.26}$	17^{+93}_{-17}			0.11	0.3	156.42/139
		66^{+12}_{-14}*	$0.69^{+0.11}_{-0.09}$				
M51	$1.70^{+0.15}_{-0.19}$	$0^{+1.6}_{-0}$	$0.71^{+0.05}_{-0.02}$	947^{+812}_{-528}	0.9	0.07	235.18/173

Notes. *This value is referred to the column obscuring the thermal component. [a]Observed 2–10 keV flux in units of 10^{-12} erg s^{-1} cm^{-2}. [b]Unobscured 2–10 keV luminosity in units of 10^{41} erg s^{-1}, corrected for absorption quoted in column 3.

Table 6. Compton-thick model.

Name	Γ	EW(eV)	A [a]	$f_{2-10\,keV}$[b]	χ^2/dof
NGC 2273	1.9f	4460^{+900}_{-3610}	$3^{+\infty}_{-1.7}$	0.62	24.88/19
NGC 3147	1.9f	548^{-508}_{+387}	$0.11^{+0.08}_{-0.09}$	0.02	267.11/282
NGC 4698	1.9f	–	$0.15^{+0.02}_{-0.01}$	0.01	245.04/250

Notes. [a]The meaning of parameter A is explained in Section 4.2. [b]Observed 2–10 keV flux in units of 10^{-12} erg s^{-1} cm^{-2}.

the 2–10 keV band, assuming that the emission is not absorbed by the torus, whereas $f_{(2-10\,keV)sc}$ is the observed flux of the fitted scattered component in the same band. Given that the scattering accounts for typically ∼1 per cent of the total X-ray emission, any value of A that is less than one suggests that we see only a small portion of the reflector, and small values mean the reflected contribution to the observed flux is almost insignificant. We apply this model to NGC 2273, 3147 and 4698, which all show low absorption. That model provides a good representation of the data for NGC 4698 ($\chi^2 = 245.04$ for 250 degrees of freedom), 2273 ($\chi^2 = 24.88$ for 18 d.o.f.) and 3147($\chi^2 = 267.11$ for 282 d.o.f.) (see also Table 6).

5 RESULTS FOR SINGLE OBJECTS

In this section we discuss the results of the spectral fits for each object in our sample individually and compare our result to previous X-ray studies. NGC 1167, 1667 and 3486 did not give sufficient counts for a full spectral analysis to be performed. We did obtain a $>3\sigma$ detection in the 2–10 keV band for both objects. Clues for the spectral shape of the sources come from their hardness ratio. Here we define hardness ratio (HR) as $(h - s)/(h + s)$, where h and s are the total number counts in the detection cells, in the 2–10 and 1–2 keV bands respectively. For our analysis we chose to use GIS data only.

5.1 NGC 1167

The hardness ratio of the source is -0.22 ± 0.12, which corresponds to a power law of $\Gamma = 2.5 \pm 0.3$ assuming Galactic absorption. This corresponds to an observed flux in the 2–10 keV band of 4.0×10^{-14} erg s^{-1} cm^{-2} and a luminosity of 2.0×10^{40} erg s^{-1}. We note that the derived spectral index is rather steeper than is typical for Seyfert galaxies, suggesting the possible presence of an additional soft component, possibly coming from a starburst region in the vicinity of the AGN.

The low $f_{HX}/f_{[O\,III]} = 0.23$ ratio (see Section 6 for a detailed discussion on the implications of this ratio) for this source would suggest a Compton-thick Seyfert 2 galaxy. On the other hand, the HR analysis showed that NGC 1167 has a steep spectrum, while in the context of a Compton-thick interpretation we would expect a flat spectrum. Unfortunately, the HR analysis only provides an indication for the spectral shape and no information about multiple components contributing to the spectrum. It is quite likely that the X-ray spectrum of NGC 1167 is complex, with different components contributing to different energies. For example, a very strong soft excess, possibly originating from intense star-forming activity, could produce a steep spectrum even if the emission from the central source is completely blocked by a Compton-thick absorption screen. However, because NGC 1167 is too faint for any further spectral analysis to be performed, the nature of its X-ray emission cannot be determined.

5.2 NGC 1667

NGC 1667 has shown a decrease of a factor of ∼150 in the 2–10 keV flux since its discovery (e.g. Polleta et al. 1996, Turner et al. 1997). The object is too faint to perform any spectral analysis. The hardness ratio of the source is -0.52 ± 0.14, which corresponds to a power law of $\Gamma = 3.2 \pm 0.4$. Assuming Galactic absorption the observed 2–10 keV flux is then $\sim 8 \times 10^{-14}$ erg s^{-1} cm^{-2}, which corresponds to a luminosity of 1.3×10^{41} erg s^{-1}. The slope is steeper than the canonical for Seyfert galaxies and, again, some fraction of the emission could be attributed to starburst emission. Indeed, Radovich & Rafanelli (1996) find evidence for star formation within 10 kpc of this source, thus favouring the latter interpretation. The low $f_{HX}/f_{[O\,III]} = 0.1$ ratio for this source would suggest that it is a Compton-thick candidate.

The substantial reduction in the hard X-ray flux over a ∼20-yr time-scale which has, presumably, not yet been reflected in the narrow-line region would provide an alternative hypothesis to explain the anomalous ratio. Indeed, assuming that the reduction in the hard X-ray flux over a ∼20-yr timescale has not yet been reflected in the narrow-line region (NLR), we find that the NLR in NGC 1667 should be located at >6 pc. Given that the NLR lies 10–100 pc from the central source, it appears that the substantial change in the hard X-ray flux has indeed not reached the NLR yet. This explanation is the most likely explanation of the low $f_{HX}/f_{[O\,III]}$ ratio and NGC 1667 is probably Compton-thin.

5.3 NGC 2273

This galaxy has been studied by Maiolino et al. (1998) using *BeppoSAX* data. They found that their data are best fitted by a Compton-thick reflection-dominated model. In addition they did not detect any emission with the PDS on board *BeppoSAX* and thus they suggested that if the Compton-thick model is valid, then the

absorbing column in our light of sight must be larger than $10^{25}\,\mathrm{cm}^{-2}$. The 'scattering' model provides a better fit to the *ASCA* data (with a column close to $10^{24}\,\mathrm{cm}^{-2}$ and an equivalent width of $\sim$500 eV), and thus is our preferred fit. It is apparent from Fig. 1 that the flat spectrum originally obtained from a simple power-law fit is caused by a turn-up in the spectrum at energies above $\sim$5 keV. Indeed, a spectral fit over the restricted 0.2–5 keV range gives a good fit to a power law with a slope of 1.5 ± 0.6, consistent with the canonical AGN and our scattering interpretation. The ratio of the unobscured hard X-ray emission to the [O III]λ5007 emission is low, indicating that we do not observe the primary emission and the Compton-thick model described in the text, yields a poor fit. It is likely that the spectrum of NGC 2273 is more complex. It is probable that a warm absorber medium and/or starburst emission contribute to the soft X-ray spectrum of this Seyfert 2, whereas the emission line around 6.4 keV could be a blend of iron lines. Unfortunately, the low quality of these data does not allow us to separate the components, which may contribute to the NGC 2273 X-ray spectrum.

5.4 NGC 3079

The *Einstein* Image Proportional Counter (IPC) detected NGC 3079 at the 3.2σ level (Fabbiano, Feigelson & Zamorani 1982), with a flux of $3.7 \times 10^{-13}\,\mathrm{erg\,s^{-1}\,cm^{-2}}$. The *ROSAT* Position Sensitive Proportional Counter (PSPC) data are dominated by a nuclear point source but emission is detected up to 2.5 arcmin from the nucleus (Reichert et al. 1994). Pietsch, Trinchieri & Vogler (1998) resolved the X-ray emission with the *ROSAT* PSPC and High Resolution Imager (HRI) into three components:

(i) extended emission in the innermost region, with $L_x = 3 \times 10^{40}\,\mathrm{erg\,s^{-1}}$, coincident with the super-bubble seen in optical images,

(ii) emission from the disc of the galaxy that can partly resolved into three point-like sources, and

(iii) very soft X-shaped emission from the halo extending to a diameter of 27 kpc.

Ptak et al. (1999) first presented the *ASCA* data for this galaxy. Their best-fit spectral parameters have large uncertainties: the power-law $\Gamma \sim 2.20^{+2.0}_{-1.0}$ and $N_\mathrm{H} \approx 6^{+4}_{-5} \times 10^{21}\,\mathrm{cm}^{-2}$. The star-forming component was described by a Raymond–Smith model with $kT = 0.14 (< 0.54)$ keV. Our analysis is in broad agreement with Ptak et al. (1999), although the spectral index is somewhat flatter. Our best-fitting model is the 'composite' one (see Table 5), although no significant iron K_α emission is detected. No variability was detected by Ptak et al. (1996), consistent with a Compton-thick scenario. Indeed, the X-ray to [O III]λ5007 ratio supports either a Compton-thick interpretation or a substantial starburst contribution. Again, NGC 3079 seems to have a complex spectrum and the nature of the X-ray emission cannot be determined with the current data.

5.5 NGC 3147

Emission in the vicinity of NGC 3147 was detected at 3σ by *HEAO* (Rephaeli, Gruber & Persic 1995), but no significant signal was detected by *Einstein*, implying a decrease in the flux between these two observations. Ptak et al. (1996) first studied this object with *ASCA*. They found that the data are well fitted by a simple power law with $\Gamma = 1.9$ and there is no indication for absorption. Our results are in excellent agreement with those of Ptak et al. (1996). Our best-fitting model is the single power law with the iron line. In principle, other more complicated models such as the scattering model or the Compton-thick model provide equally acceptable χ^2-values. In the case of the 'scattering' model we obtain a very large column of $10^{24}\,\mathrm{cm}^{-2}$ while the scattered emission is $\sim$5 per cent of the primary component. However, such high columns cannot be probed by *ASCA*, thus we do not show the model parameters for this model in Table 4. In addition, the Compton-thick model provides an equally good representation of the data statistically; here it is the scattering component which dominates the fit. The absence of variability (Ptak et al. 1999) could in principle favour such models. However, although the above models provide good fits to the data, they are rather contrived, as the *ASCA* bandpass does not allow us to constrain any models with an obscuring column higher than $\sim 10^{24}\,\mathrm{cm}^{-2}$. Indeed, a single power-law model is identical to a scattering model with $N_\mathrm{H} > 10^{24}\,\mathrm{cm}^{-2}$ in the *ASCA* band as these columns absorb most photons below 10 keV. It is therefore interesting that the [O III]λ5007 emission does not favour the above two models (composite and scattering).

5.6 NGC 3486

The hardness ratio is 0.29 ± 0.12. This corresponds to a quite flat power law of $\Gamma = 1.2 \pm 0.3$, assuming Galactic absorption, which is suggestive of high amounts of obscuration. For example, the well-known nearby Compton-thick AGNs (e.g. Circinus, NGC 1068) exhibit flat spectra below 20 keV as a result of the combination of the reflection and the scattering components. The observed flux, assuming Galactic absorption, is $\sim 5 \times 10^{-14}\,\mathrm{erg\,s^{-1}\,cm^{-2}}$.

We carried out simulations in order to determine the amount of obscuring medium needed to obtain a change of Γ from 1.9 (which is the common value for AGNs) to 1.2. We found that the source should be obscured by a column density of $N_\mathrm{H} = 3.2 \times 10^{21}\,\mathrm{cm}^{-2}$. Using $\Gamma = 1.9$ and $N_\mathrm{H} = 3.2 \times 10^{21}\,\mathrm{cm}^{-2}$ we obtain an observed flux of $\sim 5 \times 10^{-14}\,\mathrm{erg\,s^{-1}\,cm^{-2}}$, which corresponds to a luminosity of $\sim 5 \times 10^{38}\,\mathrm{erg\,s^{-1}}$. This is too low for a Seyfert galaxy, suggesting high absorption in our line of sight (but see Roberts & Warwick 2000).

The [O III]λ5007 ratio is relatively low (2.9). In order for the ratio to be comparable to the ratios observed in Seyfert galaxies (see Section 6) the source should be obscured by a column density of $\sim 1 \times 10^{24}\,\mathrm{cm}^{-2}$, assuming a power law of $\Gamma = 1.9$. This is much higher than the column derived from the HR analysis assuming $\Gamma = 1.9$. This indicates that the spectrum cannot represented by a single power-law model, and that other components contribute to the X-ray spectrum as well.

5.7 NGC 4698

NGC 4698 was observed using *Einstein*, and its 0.2–4.0 keV flux is $2.8 \times 10^{-13}\,\mathrm{erg\,s^{-1}\,cm^{-2}}$. A detailed discussion on this object is presented in Section 6.

5.8 M51

M51 is known as the 'Whirlpool galaxy'. The *Einstein* HRI detected X-ray emission from M51 with a luminosity $L_\mathrm{x} = 3.0 \times 10^{40}\,\mathrm{erg\,s^{-1}}$ in the 0.2–4.0 keV band. The emission is extended and the luminosity of a point source at the nucleus is

$L_{(0.2\text{–}4.0\,\mathrm{keV})} < 1.5 \times 10^{39}\,\mathrm{erg\,s^{-1}}$ (Palumbo et al. 1985). The *ROSAT* PSPC spectrum of the M51 nucleus is fitted with a thermal plasma of $kT \sim 0.4\,\mathrm{keV}$ (Marston et al. 1995; Read, Ponman & Strickland 1997), indicating that the AGN does not dominate the nuclear soft X-ray emission. The *ROSAT* PSPC observations revealed extended emission (Ehle, Pietsch & Beck 1995). At the hard energies the *Ginga* data are fitted with a photon index of $\Gamma = 1.4$ and an X-ray luminosity of $L_{(2\text{–}20\,\mathrm{keV})} = (1.2 \pm 0.6) \times 10^{41}\,\mathrm{erg\,s^{-1}}$ from a $\sim$1-deg^2 field containing M51 (Makishima et al. 1990). The data are also fitted with a $kT = 7\,\mathrm{keV}$ thermal bremsstrahlung model plus a power law with $\Gamma = 1.6$ absorbed by a column of $4 \times 10^{23}\,\mathrm{cm^{-2}}$. Terashima et al. (1998) analysed *ASCA* data and found extended emission from M51 in the 2–5 keV energy range. They detected a soft thermal emission represented by either $kT \sim 0.4\,\mathrm{keV}$ with low iron abundance, or by two kT plasmas ($\sim$0.3 and $\sim$0.8 keV). The hard emission is represented by a power law with $\Gamma \sim 1.4$ and $\sim$1 respectively. The fact that extended emission is observed in the 2–5 keV band clearly suggests that the AGN emission contributes only to the hardest end of the *ASCA* spectrum and is either suppressed at the softer energies or is not the dominant contributor of the energy output at these energies.

Our best-fitting model for M51 is the composite model with $kT \sim 0.7\,\mathrm{keV}$ and a spectral slope of $\sim$1.7. However, we obtained an upper limit for the column density of $1.6 \times 10^{21}\,\mathrm{cm^{-2}}$. This is not sufficient to obscure the AGN X-ray emission up to $\sim$5 keV, as it is indicated by the analysis of the brightness profile of M51. The emission could be interpreted as the superposition of thermal emission at soft energies (below 2 keV), emission from low-mass X-ray binaries (LMXBs), which contribution dominates at the 2–5 keV band and a power-law component from the AGN, which is revealed above 5 keV. In this case the active nuclei should be obscured by a column of $>5 \times 10^{23}\,\mathrm{cm^{-2}}$. However, since the AGN and the LMXBs both show a power-law spectrum of $\Gamma \sim 1.7$–1.8, it is possible that both components could be fitted as a power-law model with no need of excess absorption. On the basis of its [O III]λ5007 flux, M51 is a Compton-thick candidate. We note here that we also tried a Compton-thick model, with either two Raymond–Smith models and a reflected continuum (PEXRAV model), or a Raymond–Smith model, a power-law model to account for the possible LMXB contribution and the reflection component. However, although we obtained good fits the reflection component did not contribute in the *ASCA* band leaving the possibility where the hard X-ray emission is dominated by a scattered component more plausible in this band.

6 DISCUSSION

6.1 Are most of our objects Compton-thick ?

A couple of our objects show no evidence for intrinsic absorption. We note that in the case of poor photon statistics a Compton-thick object could be misidentified as a low-N_{H}, steep spectrum type-1 AGN, especially if the steep scattered emission dominates over the reflected component.

It is thus possible that *ASCA* only 'sees' the scattered component. Therefore, the lack of intrinsic absorption in some of our objects may indicate that these objects are Compton-thick.

Further clues on whether these AGN are Compton-thick can be given by studying the isotropic properties of the galaxy. In the case of an AGN as isotropic emission, we consider the infrared (IR) and the hard X-ray emission (in the case of Compton-thin absorption) both been able to penetrate the torus, and the [O III]λ5007 line emission produced in the narrow line region, and thus free of viewing angle effects. Indeed, Alonso-Herrero et al. (1997) showed that the 2–10 keV to [O III]λ5007 and IR flux ratios are comparable for obscured and unobscured AGNs. The advantage of studying isotropic properties then, is that they act as an indicator of the strength of the nuclear source. Maiolino et al. (1998) have proposed that the measurement of the observed hard X-ray flux (2–10 keV) against the [O III]λ5007 flux is indeed a powerful diagnostic. Moreover, although the line is emitted on the NLR scales, the host galaxy disc might obscure part of the NLR and should be corrected for the extinction deduced from the Balmer decrement (Maiolino & Rieke 1995). The corrected [O III]λ5007 flux is given by the following relation (Bassani et al. 1999):

$$F_{[\mathrm{O\,III}]\mathrm{cor}} = F_{[\mathrm{O\,III}]\mathrm{obs}}[(\mathrm{H}_\alpha/\mathrm{H}_\beta)/(\mathrm{H}_\alpha/\mathrm{H}_\beta)_0]^{2.94} \quad (1)$$

Assuming an intrinsic Balmer decrement $(\mathrm{H}_\alpha/\mathrm{H}_\beta)_0 = 3$. All the well studied Seyfert 1 galaxies have $f_{\mathrm{HX}}/f_{[\mathrm{O_{III}}]} \geqslant 1$ (Maiolino 1998). An absorption of less than a few times $10^{23}\,\mathrm{cm^{-2}}$ will lower this ratio by a factor of $\sim$5 with respect to Seyfert 1s. When $N_{\mathrm{H}} > 5 \times 10^{24}\,\mathrm{cm^{-2}}$, the reduction is about two orders of magnitude. The flux ratios are presented in Table 7. For each object we use the flux derived using the most plausible model. Of course we have to be cautious, as there may be some limitations on the use of the [O III]λ5007 flux ratio as an indicator of the unobscured X-ray emission. Indeed, in cases where the ionization-cone axis lies perpendicular or close to the minor axis there might be lack of ionized gas. Then the [O III]λ5007 flux may not be a good indicator of the nuclear strength. However, the disc height for a typical spiral galaxy is of the order of $\sim$100 pc, whereas the size of the region where the bulk of the [O III]λ5007 flux is produced is of a similar size. Thus it is most likely that the relative orientation of the nuclear accretion to the host galaxy disc will not significantly affect the [O III]λ5007 flux. Another caveat that we should take into account is if the torus hides the innermost regions of the NLR from our view, and thus the observed [O III]λ5007 is lower than the actual flux produced. Again, the small inferred size of the torus (a few pc) relative to the size of the NLR (kpc scale) implies that such an effect does not significantly affect the above ratio. In addition, Mulchaey et al. (1994) compared the properties of samples of Seyfert 1 and Seyfert 2 galaxies, and showed that the ratio of the [O III]λ5007 emission to the unobscured hard X-ray emission is the same for both types of galaxies, indicating that the [O III]λ5007 flux cannot be obscured by the torus. In the case of the IR emission, caution must be taken because the IR emission may be contaminated by starburst emission, particularly in the case of low-luminosity AGN where the star formation in the host galaxy dominates the emission. Multiwavelength observations of our objects have shown that some of them indeed contain starburst activity (see Section 5). Therefore we choose not to apply this criterion to our data.

In Table 7 it is noted whether the object is Compton-thin or Compton-thick, on the basis of both the X-ray spectral analysis and the $f_{\mathrm{HX}}/f_{[\mathrm{O_{III}}]}$ ratio. It is clear that in some cases there is a discrepancy between the classifications inferred from the spectrum and the $f_{\mathrm{HX}}/f_{[\mathrm{O_{III}}]}$ ratio. It is likely that the X-ray spectrum of Seyfert 2 galaxies and especially those with high column densities, where the medium and hard X-ray photons are suppressed, and emission from the host galaxy, circumnuclear starburst and warm absorbers significantly contributes to the spectrum. The present (*ASCA*) data does not allow us to distinguish the contribution of these components.

Table 7. Flux ratios.

Name	f_{HX} [a]	f_{HX} [b]	$f_{[O_{III}]}$ [c]	$f_{HX}/f_{[O_{III}]}$ [d]	$f_{HX}/f_{[O_{III}]}$ [e]	Type[f]	Type[g]
NGC 1167	0.04	0.04	17	0.23	0.23		CT
NGC 1667	0.08	0.08	197	0.04	0.04		CTn
NGC 2273	1.11	3.65	277	0.40	1.32	CTn	CT
NGC 3079	0.11	1.10	90	0.11	1.20	CTn	CT
NGC 3147	1.63	1.64	9.0	18.11	18.22	CTn	CTn
NGC 3486	0.05	0.05	1.7	2.94	2.94		CT/CTn
NGC 4698	1.04	1.10	2.0	52	55	CTn	CTn
M51	0.11	0.55	150	0.07	0.37	CTn	CT

Notes. [a] 2–10 keV observed flux in units of 10^{-12} erg s^{-1} cm^{-2}. [b] 2–10 keV unobscured flux in units of 10^{-12} erg s^{-1} cm^{-2}, using the most plausible model for each object. [c] Corrected [O III]λ5007 flux in units of 10^{-14} erg s^{-1} cm^{-2}, taken from Risaliti et al. 1999. [d] Using the observed 2–10 keV flux. [e] Using the absorption corrected 2–10 keV flux for the most plausible model for each object. [f] Whether the object is Compton-thin (CTn) or Compton-thick (CT) after taking into consideration the spectral fitting. [g] Whether the object is CTn or CT after taking into consideration the $f_{HX}/f_{O_{[III]}}$ ratio.

Summarizing, NGC 1167, 2273, 3079, and M51 are Compton-thick candidates according to their $f_{HX}/f_{[O_{III}]}$ ratio. The are best for the three of them (NGC 2273, 3079, and M51) are best fitted with a highly obscured ($N_H \sim 10^{23}$–10^{24} cm^{-2}) power law. However, because of large uncertainties in the derived column density, we were not able to distinguish between the Compton-thin and Compton-thick interpretations. This may be a result of the underlying complexity of the X-ray spectra as shown more clearly in the case of M51. However, the current data, especially in the case of NGC 2273, are only sufficient to support analyses with simplistic models. NGC 3486 is probably a heavily obscured Seyfert 2 galaxy. Both NGC 3147 and 4698 have high $f_{HX}/f_{[O_{III}]}$ ratios, comparable to the value obtained by Alonso-Herrero et al. (1997), if we take into account the extinction in the NLR, which clearly shows that the 2–10 keV X-ray emission is not affected by absorption.

6.2 Seyfert 2 galaxies with no absorption in X-rays: the case of NGC 4698

The most striking example from our low absorption Seyfert 2 is NGC 4698. The X-ray data do not require absorption and the alternative hypothesis of Compton thickness was ruled out on the basis of the [O III]λ5007 flux. Further evidence for the amount of obscuring material can be obtained by the iron-line emission. For Compton-thin Seyfert 2 galaxies the average equivalent width (EW) value derived from *ASCA* data is 363 ± 254 (Gilli et al. 1999), whereas for Compton-thick objects the equivalent width can be well above 1 keV (e.g. for NGC 6240, the iron K_α line has an EW ∼ 1.58 keV). However, we do not obtain a significant detection of line emission but can only set a 90 per cent upper limit on the equivalent width of such a feature of 425 eV. This value is too low for a Compton-thick object, and in that sense the Compton-thick interpretation for this object can be ruled out.

NGC 4698 is not the first Seyfert 2 galaxy found which shows no intrinsic absorption. Ptak et al. (1996) first studied NGC 3147 (which is also included in our sample) with *ASCA* in the context of an AGN. They interpreted its X-ray emission as originating in a Seyfert 1 (no Seyfert classification was available at that time) or a heavily obscured Seyfert 2. Moreover, Bassani et al. (1999) showed that NGC 7590 has negligible absorption in X-rays as well, although classified as a Seyfert 2 galaxy. Using the [O III]λ5007 criterion, the latter authors ruled out the Compton-thick possibility for both objects and suggested that these lack a broad-line region (BLR), so their appearance as Seyfert 2 is intrinsic and not a result of absorption. Thus optical classification as type 2 objects will be explained by the presence of narrow emission lines only as a result of a lack of the broad-line region.

Many models for the formation of broad-line clouds argue towards a link to the disc (see Collin-Souffrin 1987 and Witt, Czerny & Zycki 1997), thus the existence of a class of objects without a BLR would set constraints on the conditions under which a BLR is formed, as well as the properties of the disc. In particular, Nicastro (2000) recently presented a model in which a standard accretion disc accreting at low rates is not expected to produce broad emission lines. According to this model a vertical disc wind, originating at a critical distance in the accretion disc, is the origin of the broad-line emission region. The disc wind forms for external accretion rates higher than a minimum value $\dot{m}_{min}$ below which a standard disc is stable. For accretion rates $\dot{m} > \dot{m}_{min}$, the disc is unstable and a stabilizing, co-accreting 'disc/corona+wind' system forms. The minimum accretion rate is $\dot{m}_{min} \simeq 0.3n(am)^{-1.8}$, where $n = 0.06$ is the efficiency of the accretion, $a = 0.1$ is the viscosity coefficient and m is the mass of the black hole. This gives a minimum accretion rate of $\dot{m} > \dot{m}_{min} \sim (1\text{–}4) \times 10^{-3}$ for m in the range 10^6–10^9 $M_\odot$. Providing that the accretion rate in NGC 4698 is low, this model explains the absence of broad emission lines. Assuming that the mass of the black hole residing in NGC 4698 is the typical 10^6 $M_\odot$ for Seyfert galaxies, the X-ray luminosity in the 2–10 keV energy band (2.2×10^{40} erg s^{-1}) is ∼3 orders of magnitude lower than the observed X-ray luminosities (∼10^{43} erg s^{-1}) in Seyfert 1 galaxies. This discrepancy could easily be attributed to a lower accretion rate, which immediately explains the absence of broad emission lines in the spectrum of NGC 4698.

The lack of column density could also be explained by the presence of a dusty warm absorber. The presence of dust accounts for the optical obscuration of the broad-line region, whereas the lack of X-ray absorption is caused by the ionization state of the absorber. In such a case cold absorption is no longer required. We note here that when we discuss dusty warm absorber models we should consider that there are two grain-destruction mechanisms that must be taken into account. First, the sublimination of the grains when they become too hot (∼2000 K) and secondly, thermal sputtering, which destroys the dust once the gas electron temperature reaches 10^6 K (Draine & Salpeter 1979; Laor &

Draine 1993). Assuming that the warm absorber is photoionized, the gas temperature in a typical warm absorber where oxygen is highly ionized is only $T \sim 5 \times 10^4$ K and thermal sputtering is negligible. If collisional ionization plays a significant role, then $T \sim 10^6$ K and the dust will be destroyed. However, Reynolds et al. (1997) showed that photoionization dominates the ionization of the plasma unless $r \geq 100$ pc, where r is the distance of the warm absorber from the central engine. In this case a dusty warm absorber model is viable. Komossa & Bade (1998) predicted the presence of a carbon edge at 0.28 keV and showed that the dusty warm absorber smoothes the oxygen edges, making it difficult to be detected. Unfortunately *ASCA* is not sensitive enough at these soft energies, and we cannot test an actual dusty warm absorber model for our data. As at energies above 0.3 keV both the dusty warm absorber and the warm absorber are expected to imprint similar spectral features in the spectrum and because the X-ray photons are not affected by the dust, we fit our data in the energy range 0.5–10 keV with a warm absorber model in order to examine the possibility of the presence of ionized material in the very central region of NGC 4698. Although we obtain a good fit to the data ($\chi^2 = 244.8$ for 265 d.o.f), the ionization parameter of the warm material is unphysically high, implying that the data do not require any kind of absorption. Further clues on the nature of this galaxy can be given by looking for short-time variability in the 2–10 keV band. The data do not show evidence for variability, however we note that this could simply be caused by our limited photon statistics.

An insight into the energy production mechanisms at different wavebands can come from the spectral energy distribution (SED) of the galaxies. The SED for NGC 4698 (Fig. 2, stars) reveals an unexpected emission distribution compared to the median radio-quiet (Fig. 2, solid line) SED of Elvis et al. (1994). For comparison we also show the SED of the archetypal Compton-thick Seyfert 2 galaxy NGC 1068 (Fig. 2, squares). It is clear that the NGC 4698 SED deviates from both the typical and the Compton-thick AGN SEDs. The latter confirms our analysis that NGC 4698 is not a Compton-thick Seyfert 2 galaxy.

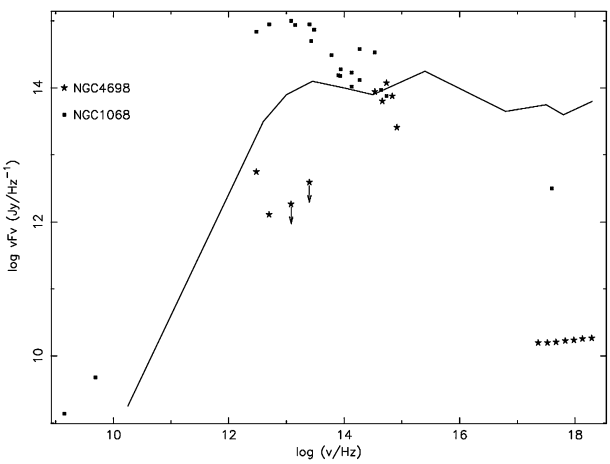

Figure 2. The NGC 4698 SED (star symbols). The fluxes are taken from NED. Where there are multiple observations, we used data obtained using the smallest aperture. Specifically, *V*-band magnitude 11.39 (64.9-arcsec aperture), *I*-band magnitude 10.54 (36-arcsec aperture) and *H*-band magnitude (51.8-arcsec aperture), for comparison we also show the NGC 1068 SED (square symbols) and the median SED (line) from Elvis et al. (1994).

To investigate the differences we computed the 'optical/X-ray' spectral index (Tananbaum et al. 1974) α_{ox} between 2500 Å and 2 keV, which is defined as: $\alpha_{ox} = -0.384 \log [F_\nu(2\,\mathrm{keV})/F_\nu(2500\text{Å})]$. As there are no measurements in the UV, we made the conservative assumption that there is no UV bump and we extrapolate from the optical into the UV as a straight line in the νF_ν space. Then $\alpha_{ox} \sim 2.5$. Typically it is found that $\alpha_{ox} \sim 1.4$ for AGNs. It is evident that NGC 4698 is relatively weak in the X-ray. However, as has already been shown, there is evidence that the weakness is intrinsic and nota result of absorption, unless the UV and or X-ray emissions vary significantly. We then computed the IR/HX ratio as defined by Mulchaey et al. (1994) and obtained ~1.5. This is an upper limit because the flux at 25 μm is an upper limit. However, it is clear that the ratio is comparable to that of Seyfert galaxies (Mulchaey et al. 1994). The discrepancy between the SED of NGC 4698 and that of other AGNs could be explained by either an excess in the optical emission or by a deficit in both the IR and X-ray emission. However, caution must be taken in interpreting the SED, as the measurements have been taken at different epochs and using different apertures.

6.3 The distribution of absorbing columns and the implications for the X-ray background

The X-ray background is believed to be produced by the superposition of discrete sources. In the soft band, at a flux limit of 1×10^{-15} erg cm^{-2} s^{-1}, the dominant population are broad-line AGNs (Hasinger et al. 1998). *ASCA* resolved only ~30 per cent of the 2–10 keV XRB into discrete sources (Georgantopoulos et al. 1997), the majority of which are again broad-line AGNs. However, broad-line AGNs have power-law spectra with a photon index of $\Gamma \sim 1.9$ (Nandra & Pounds 1994), which is significantly softer than that of the CXB in that band (~1.4; Gendreau et al. 1995). Thus there must be a large number of undetected objects which have harder X-ray spectra than the local broad-line AGNs. This population should be obscured because it does not come up in the softer energies.

The deep *Chandra* surveys deepened the riddle of the origin of the XRB even further. In the hard 2–10 keV band, they probed fluxes at least an order of magnitude deeper than *ASCA* (Mushotzky et al. 2000), albeit with limited number statistics because of the small field-of-view of Advanced CCD Imaging Spectrometer (ACIS) onboard *Chandra*. A large fraction of the detected sources is associated with quasi-stellar objects (QSOs) which appear to have steep spectra. Surprisingly, no numerous, clear-cut examples of the putative obscured AGN population at high redshift have yet been found. Instead, two 'new' populations emerged which are associated with either early-type galaxies or extremely faint optical counterparts.

All the current models which try to reconstruct the X-ray background spectra utilize a population of objects with an underlying spectral index equivalent of those of unobscured AGNs and a range of obscuring columns. Observational support for such a model comes from the detection in deep *ROSAT* surveys (Boyle et al. 1995) of a large number of faint X-ray sources whose optical counterparts are galaxies with narrow lines only. Thus these galaxies are considered to be that 'obscured' AGN population. In addition, the lack of a population with spectral index similar to the X-ray background again indicates that a large population of heavily obscured AGN should emerge at hard energies.

Our analysis suggests that simple models cannot describe the spectra of the Seyfert 2 galaxies adequately. Especially in the case

of heavily obscured or Compton-thick objects, where the medium and/or hard X-ray emission is suppressed and emission from the host galaxy, circumnuclear starbursts and/or warm absorbers contributes significantly and imprints features on the spectrum. Also, surprisingly, two of our Seyfert 2s (NGC 3147 and 4698) do not show evidence for absorption above the Galactic level. It becomes evident that the complexity of the Seyfert 2 spectrum should be taken into account when constructing models for the synthesis of the X-ray background.

In addition, latest results from *ASCA* and *BeppoSAX* (Pappa et al. 2001 and Comastri et al. 2001, respectively) show that there is a population of objects at high redshifts, with broad lines in the optical region which have high amounts of X-ray absorption. All the above results suggest that the distribution of column densities is complex, and one cannot use a simple recipe for the $N_{\rm H}$ distribution. The compilation of large optically selected or IR selected Seyfert 2 samples and the determination of the X-ray spectrum of Seyfert 2 galaxies, as well as the study of obscured AGN at high redshift, will shed new light on the X-ray background synthesis models.

7 CONCLUSIONS

We have presented a systematic analysis of eight bona fide Seyfert 2 galaxies. We selected sources from the Ho et al. (1997) spectroscopic sample of nearby galaxies. We included all the brightest [O III]λ5007 Seyfert 2 galaxies, for which X-ray data were or recently became available. Our uniform analysis showed that, in general, our objects show a complex X-ray spectrum. On the basis of the [O III]λ5007 flux, the Compton-thick possibility was ruled out for two of our low-absorption objects, namely NGC 3147 and 4698, leaving open questions as to the nature of these objects. We propose that the deficit in absorption may be caused either by the presence of a dusty warm absorber or by the lack of broad-line region. In the latter case the Seyfert 2 appearance is intrinsic and an absorption medium is no longer required. Furthermore, for NGC 2273, spectral analysis favours the scattering model. However, the column density could not be constrained, thus we could not distinguish between the Compton-thin and Compton-thick interpretations. Yet its [O III]λ5007 flux is too low, and favours the Compton-thick interpretation. In the case of M51, where the reflection-dominated Compton-thick model is not favoured by the data but its $f_{\rm HX}/f_{\rm [O\,III]}$ is low, we argue that the discrepancy may be explained either by a warm scatter model for the hard X-ray emission, or by optical or X-ray variability. Finally, we suggest that the above results may be important in the study of the X-ray background, because all the current XRB synthesis models utilize a population of objects with an underlying spectral index equivalent to that of unobscured AGNs and a range of obscuring columns, whereas our results suggests that there are type 2 objects with spectra quite untypical of the ones expected and that the X-ray spectrum is composed by several components (which should be taken into account when constructing such models). Discovery of more Seyfert 2 galaxies with spectra distinct to the 'nominal' Seyfert 2 spectra will show whether these objects contribute significantly to the X-ray background or not, while *XMM-Newton* observations of Seyfert 2 galaxies will allow us to determine the spectral components contributing to the total X-ray spectrum and *Chandra* observations will allow us to deconvolve any extended emission.

ACKNOWLEDGMENTS

The authors thank the referee R. Maiolino for useful comments and suggestions. AP thanks Prof. M. Ward for useful discussions and K. Anagnostou for his useful help throughout the writing of this paper. This research has made use of data obtained through the High Energy Astrophysics Science Archive Research Center Online Service, provided by the NASA/Goddard Space Flight Center, the LEDAS online service, provided by the University of Leicester, and the NASA/IPAC Extragalactic Database (NED) which is operated by the Jet Propulsion Laboratory, California Institute of Technology, under contract with the National Aeronautics and Space Administration.

REFERENCES

Alonso-Herrero A., Ward M. J., Kotilainen J. K., 1997, MNRAS, 291, 557
Antonucci R., 1993, ARA&A, 31, 473
Bassani L., Dadina M., Maiolino R., Salvati M., Risaliti G., della Ceca R., Matt G., Zamorani G., 1999, ApJS, 121, 473
Boyle B. J., McMahon R. G., Wilkes B. J., Elvis M., 1995, MNRAS, 272, 462
Collin-Souffrin S., 1987, ApJ, 179, 60
Comastri A., 2001, in Proc. Conf. X-ray Astronomy 1999, Stellar Endpoints, AGNs and the Diffuse X-ray background. Pre-print (astro-ph/0003437)
Comastri A., Setti G., Zamorani G., Hasinger G., 1995, A&A, 296, 1
Dickey J. M., Lockman F. J., 1990, ARA&A, 28, 215
Draine B. T., Salpeter E. E., 1979, 231, 438
Ehle M., Pietsch W., Beck R., 1995, A&A, 295, 289
Elvis M. et al., 1994, ApJS, 95, 1
Fabbiano G., Feigelson E., Zamorani G., 1982, ApJ, 256, 397
George I. M., Turner T. J., Netzer H., Nandra K., Mushotzky R. F., Yaqoob T., 1998, ApJS, 114, 73
Georgantopoulos I., Stewart G. C., Blair A. J., Shanks T., Griffiths R. E., Boyle B. J., Almaini O., Roche N., 1997, MNRAS, 291, 203
Gendreau K. C. et al., 1995, PASJ, 47, L5
Gilli R., Comastri A., Brunetti G., Setti G., 1999, New Astron., 4, 45
Hasinger G., Burg R., Giacconi R., Schmidt M., Trumper J., Zamorani G., 1998, A&A, 329, 482
Ho L. C., Filippenko A. V., Sargent W. L. W., Peng C. Y., 1997, ApJS, 112, 391
Komossa S., Bade N., 1998, A&A, 331, L49
Laor A., Draine B. T., 1993, ApJ, 402, 441
Makishima K., Ohashi T., Kondo H., Palumbo G. G. C., Trinchieri G., 1990, ApJ, 365, 159
Maiolino R. et al., 1998, A&A, 338, 781
Maiolino R., Rieke G. H., 1995, ApJ, 454, 95
Maiolino R., Ruiz M., Rieke G. H., Keller L. D., 1995, ApJ, 446, 561
Marston A. P., Elmegreen D., Elmegreen B., Forman W., Jones C., Flanagan K., 1995, ApJ, 438, 663
Matt G. et al., 1997, A&A, 325, 13
Matt G. et al., 1999, A&A, 341, 39
Morrison R., McCammon D., 1983, ApJ, 270, 119
Mulchaey J. S., Koratkar A., Ward M. J., Wilson A. S., Whittle M., Antonucci R. J., Kinney A. L., Hurt T., 1994, ApJ, 436, 586
Mushotzky R. F., Cowie L. L., Barger A. A., Arnaud K. A., 2000, Nat, 404, 459
Nandra K., Pounds K., 1994, MNRAS, 268, 405
Nicastro F., 2000, ApJ, 530, L65
Palumbo G. C. C., Fabbiano G., Trinchieri G., Fransson C., 1985, ApJ, 298, 259
Pappa A., Stewart G. C., Georgantopoulos I., Griffiths R. E., Boyle B. J., Shanks T., 2001, MNRAS, in press (astro-ph/0105125)
Pietsch W., Trinchieri G., Vogler A., 1998, A&A, 340, 351
Polletta M., Bassani L., Malaguti G., Palumbo G. G. C., Caroli E., 1996, ApJS, 106, 399
Ptak A., Yaqoob T., Serlemitsos P. J., Kunieda H., 1996, ApJ, 459, 542
Ptak A., Yaqoob T., Mushotzky R., Serlemitsos P., Griffiths R., 1998, ApJ, 501, L37

Ptak A., Serlemitsos P. J., Yaqoob T., Mushotzky R., 1999, ApJS, 120, 179
Radovich M., Rafanelli P., 1996, A&A, 306, 97
Read A. M., Ponman T. J., Strickland D. K., 1997, MNRAS, 286, 626
Reichert G. A., Mushotzky R. F., Filippenko A. V., 1994, in Schlegel E. M., Petre R., eds, Proc. AIP Conf. Vol. 313, The Soft X-ray Cosmos. Am. Inst. Phys., New York, p. 85
Rephaeli Y., Gruber D., Persic M., 1995, A,A, 300, 91
Reynolds C. S., Ward M. J., Fabian A. C., Celotti A., 1997, MNRAS, 291, 403
Risaliti G., Maiolino R., Salvati M., 1999, ApJ, 522, 157
Roberts T. P., Warwick R. S., 2000, MNRAS, 315, 98
Sandage A., Tammann G. A., 1981, A Revised Shapley-Ames Catalog of Bright Galaxies. Carnegie Institution of Washington, Washington
Smith D., Done C., 1996, 280, 355
Tanaka Y. et al., 1995, Nat, 275, 659
Tananbaum H. et al., 1974, ApJ, 234, L9
Terashima Y., Ptak A., Fujimoto R., Itoh M., Kunieda H., Makishima K., Serlemitsos P. J., 1998, ApJ, 496, 210
Tran H. D., 1995, ApJ, 440, 565
Turner T. J., Pounds K. A., 1989, MNRAS, 240, 833
Turner T. J., George I. M., Nandra K., Mushotzky R., 1997, ApJS, 113, 23
Ueno S., Law-Green S. D., Awaki H., Koyama K., 1998, in Koyama K., Kitamoto S., Itoh M., eds, Proc. IAU Symp. 188, The Hot Universe. Kluwer, Dordrecht, p. 7
Witt H. J., Czerny B., Zycki P. T., 1997, MNRAS, 286, 848
Yaqoob T. et al., 1997, The *ASCA* ABC Guide v. 2.0. Goddard Space Flight Center, Washington, MD

This paper has been typeset from a TEX/LATEX file prepared by the author.